UNIFIED FRAMEWORK FOR AEROSERVOELASTIC RESPONSE AND STABILITY ANALYSIS, DESIGN AND TESTING

Moti Karpel

Technion – Israel Institute of Technology,
Haifa, 32000, Israel, _karpel@technion.ac.il_

Keywords: aeroelasticity, aeroservoelasticity, loads.

Abstract: Frequency-domain linear aeroservoelastic (ASE) equations of motion, with a unified application in dynamic response to gust, control commands and direct force applications, are presented. The increased-order modeling (IOM) approach is then used to complement the linear solutions with nonlinear effects. The resulting process, implemented in the Dynresp framework software, is demonstrated in various industrial applications and research projects. The parametric flutter margin (PFM) method, based on adding a reference parameter that expands the system stability range, is applied with virtually the same response formulation for linear and nonlinear stability analysis. The more general MIMO version of PFM is shown to be very useful in design studies and overall stability characteristics. The SISO version, however, is shown to be more practical and intuitive as it is based on direct response functions. The computation framework facilitates for convenient inclusion of morphing scenarios and rapid changes in flight conditions using the nonlinear time-domain block. Promising applications to flutter flight tests and high-fidelity fluid-structure interaction are presented.

1 INTRODUCTION

The dynamic aeroservoelastic (ASE) response and stability characteristics have primary effects on the design and testing of flight vehicles. Most intensive ASE calculations in industrial environment are for dynamic loads, aimed at the definition of critical load distributions for structural design, and for flutter onset conditions, aimed at ensuring that destructive flutter does not occur in the flight envelope plus safety margins. While most ASE design and certification calculations are performed using linear frequency-domain models, increasing portions require adequate evaluation of nonlinear aerodynamic, structural or control-system effects. An Increased-Order Modeling (IOM) methodology was developed for this purpose and presented a few years ago [1, 2]. It started as a practical and efficient approach to the modeling of dynamic systems that are mostly linear, but their behavior may be significantly affected by nonlinearities. The approach is based on the augmentation of a main linear block with feedback loops that represent the system nonlinearities. This paper relates mainly to the recently developed IOM-based Dynresp framework code for numerical nonlinear ASE response simulations and stability analysis. The framework makes use of common frequency-domain aeroelastic response methods and facilitates the addition of time-domain control, aerodynamic, structural and actuator nonlinearities in a systematic feedback architecture. The Dynresp code has been applied to all aspects of dynamic loads analysis at Airbus D&S [3] since 2007, and by other companies and research institutes [4].

A new Parametric Flutter Margin (PFM) method [5] for response-based flutter analysis was recently added to the IOM concept. Being based on a single stabilizing parameter, such as a certain modal damping value or discrete mass that enhances the ASE stability, the PFM method facilitates very efficient massive sensitivity studies with respect to selected stabilizing parameters [6]. Furthermore, it facilitates safer flutter tests where flutter or nonlinear limit-cycle oscillation (LCO) boundaries of a certain configuration are positively identified while actually testing a more stable configuration [7]. Two proof-of-concept wind-tunnel tests have already been performed [8,9] with very encouraging results. The stability analyses that supported the design studies and flutter tests were based on the basic IOM response formulation where the stabilizing parameter appears as a gain that closes a single-input-single-output (SISO) feedback loop.

The purpose of this paper is to provide an overall description of the IOM method and its use in the Dynresp framework, using a unified formulation and application to ASE analysis, design and testing. The application of the IOM methodology in Dynresp and its integration in the ASE response and aircraft loads calculation scheme are briefly described in Section 2. The unified formulation for linear and nonlinear dynamic response to gusts, control commands and direct forces is outlined in Section 3. The expansion of the ASE response formulation to stability analysis and sensitivity to design variables and element nonlinearities is outlined in Section 4. Applications of Dynresp in aerodynamic morphing scenarios and in CFD-based linear and nonlinear response and stability analyses are discussed in Section 5. The use of the PFM method in wind-tunnel and flight tests with enhances safety is discussed in Section 6 and conclusions are given in Section 7. Numerical examples, mostly taken from previous works, are given along the mentioned sections to demonstrate the process.

2 INCREASED-ORDER-MODELING METHODOLOGY IN DYNRESP

The IOM approach and the Dynresp framework present a systematic methodology and computational tools that exploit the numerical advantages in dealing with linear systems while keeping the complexity of the added nonlinear elements as low as required for obtaining adequate accuracy. The method, schematically depicted in Fig. 1, is based on a main linear block that is stable when disconnected from the nonlinear elements, and a nonlinear element that expresses all the nonlinearities as feedback loops. The additional CFD-related block is an example of user-defined functions (UDF) that can be added by the user to perform a particular nonlinear simulation, fluid-structure interaction (FSI) in this example. The various features of the FSI block are discussed in Section 5 below.
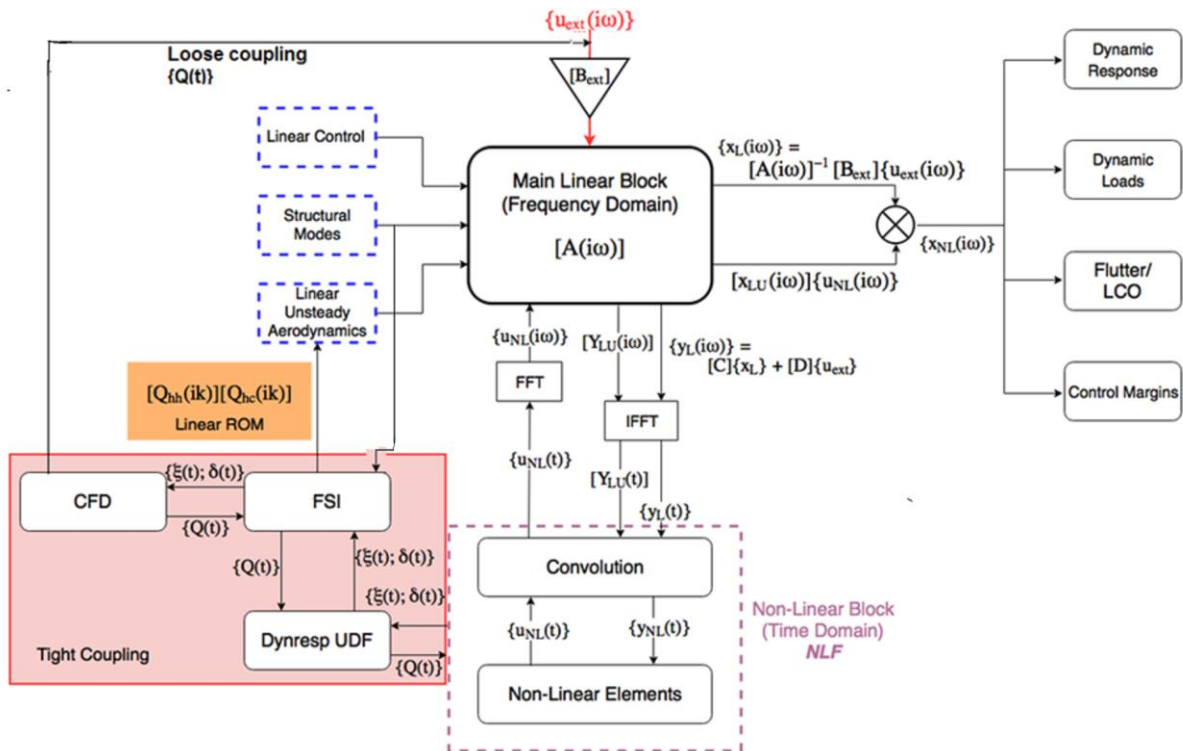

Figure 1: IOM block diagram with CFD-based data.

The response calculations are performed in 3 stages: (a) response of the linear block with the nonlinear block disconnected; (b) addition of nonlinear effects using nonlinear elements and convolution integrals; and (c) complementary response of the linear block to inputs from the nonlinear block to generate the final output. The main features of Dynresp-v12 are:
- Dynamic response to gust, maneuver-command and direct-force excitations.
- Flutter, limit-cycle oscillations (LCO) and control stability margins.
- Deterministic and stochastic excitations in all disciplines.
- Modal structural data from finite-element codes.
- Efficient structural changes and accommodation of fictitious masses.
- Unsteady aerodynamics from panel-based or linearized-CFD codes.
- Most general control and mechanical feedback architecture.
- Structural, aerodynamic and control nonlinearities.
- Modal coupling and morphing scenario.
- Summation-of-Force and Mode-Displacement loads.
- Coupling with high-fidelity nonlinear solvers.

The integration scheme of Dynresp with other codes and databases at Airbus D&S [3] is shown in Figure 2.
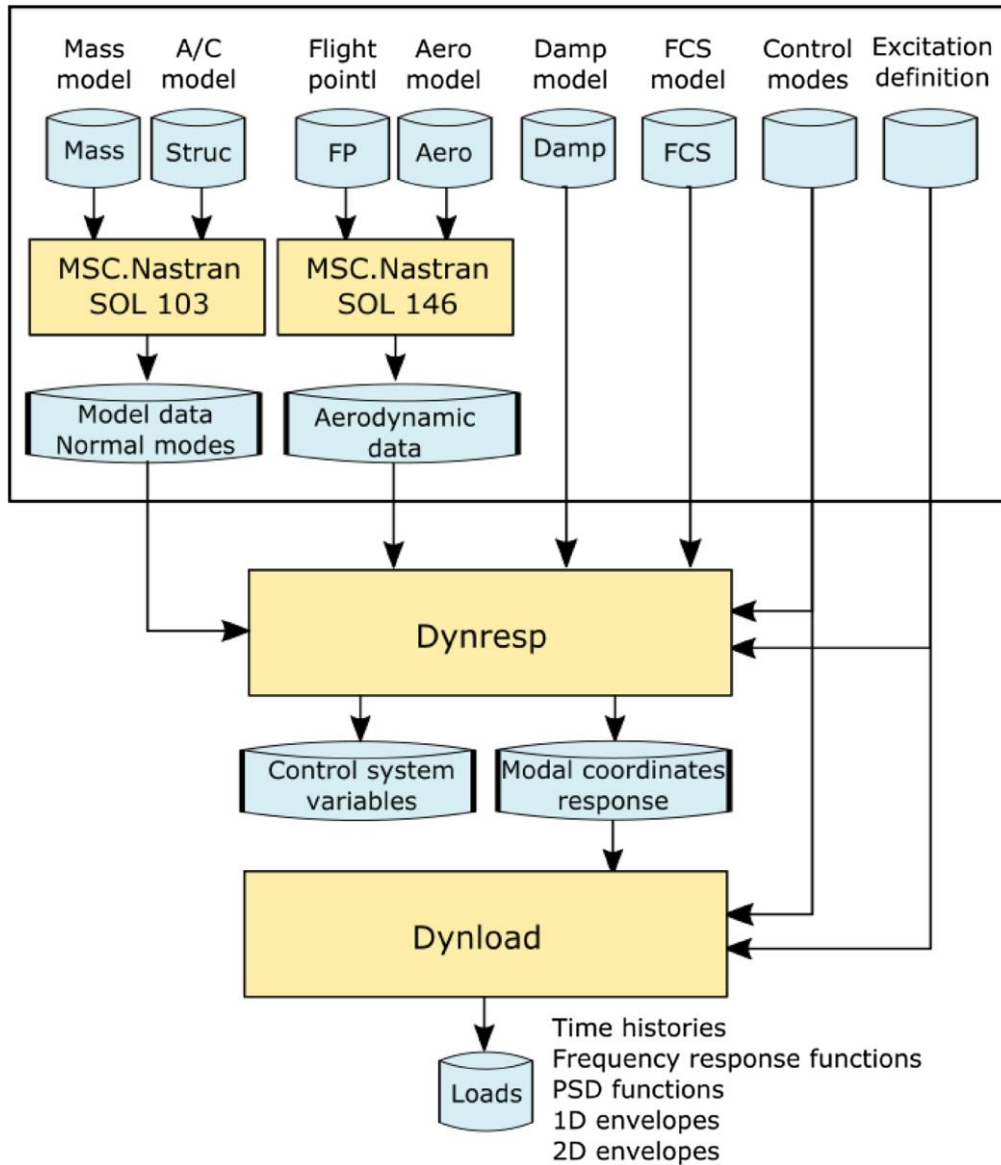

Figure 2: ASE response and aircraft loads calculation scheme

3 UNIFIED AEROSERVOELASTIC RESPONSE FORMULATION

The first IOM stage is performed in the linear block in Fig. 1. The vehicle FD equation of motion with gust, maneuver and direct-force external excitations, plus excitations from the nonlinear block, is

$$[A(i\omega)]\{x_L(i\omega)\} = \{B_G(i\omega)\}\frac{w_G(i\omega)}{V} + [B_M]\{u_{vM}(i\omega)\} + [B_D]\{F_D(i\omega)\} + [B_{NL}]\{U_{NL}(i\omega)\} \quad (1)$$

where $\{x_L(i\omega)\}$ is the FD vector of modal displacements, linear control-system states and actuator states, $[A(i\omega)]$ is the closed-loop linear system matrix. $w_G(i\omega)/V$ is the induced gust

angle of attack at a reference point, that can be replaced with a general 3D wake excitation [9]. $\{u_{vM}(i\omega)\}$ is the vector of simultaneous maneuver commands applied in terms of control inputs or direct control forces. $\{F_D(i\omega)\}$ is the vector of simultaneous direct forces, in discrete or generalized coordinates. $\{U_{NL}(i\omega)\}$ is the vector of inputs from the nonlinear block whose numerical values are not known at this stage. Detailed description of the matrices and vectors of Eq. (1) is given in [2]. The generic response to terms $\{u_{ext}(i\omega)\}$ in the right side of Eq. (1), except for the $\{U_{NL}(i\omega)\}$ term, is

$$\{x_L(i\omega)\} = [A(i\omega)]^{-1}[B_{ext}(i\omega)]\{u_{ext}(i\omega)\} \tag{2}$$

where $[B_{ext}(i\omega)]$ is the input distribution matrix. $\{u_{ext}(i\omega)\}$ is obtained via Fast Fourier Transform (FFT) of the input signal $\{u_{ext}(t)\}$. The $\{y_L(i\omega)\}$ outputs of the linear block in Fig. 1, which are inputs to the nonlinear block, can be generally expressed as

$$\{y_L(i\omega)\} = [C(i\omega)]\{x_L(i\omega)\} + [D(i\omega)]\{u_{ext}(i\omega)\} \tag{3}$$

where the coefficient matrices, $[C]$ and $[D]$, are related to modal displacements and direct-force effects (in the case of acceleration outputs). Other FD response functions are calculated in the linear block in preparation for the subsequent interaction with the nonlinear block.

The singularity of the aeroelastic system matrix in free flight at zero frequency, $[A(0)]$, does not allow a direct solution for the various $\{X(0)\}$ vectors. Dynresp provides four options for overcoming this difficulty [11]. The first option avoids the zero-frequency solution and defines the FD $\{X(0)\}$ such that the resulting TD solution, obtained by IFFT, starts at $\{x(0)\} = \{0\}$, while the FD velocity and acceleration responses at zero frequency are set to zero. The second option starts with the first one and then modifies the initial rigid-body pitch and yaw angles at zero frequency to yield zero rigid-body incidence angles (α and β), which yields zero initial loads. The third option transforms Eq. (1) at zero frequency to flight mechanics variables in a way that removes the singularity problem [11]. The forth option starts by calculating the TD modal accelerations using FFT, and then obtains the modal velocities and displacements by numerical integration, starting at their zero values.

Frequency response functions (FRFs) of the state vectors $\{x_L(i\omega)\}$ to unit inputs in $\{U_{NL}(i\omega)\}$ from the nonlinear block are arranged in the $[x_{LU}(i\omega)]$ matrix and calculated by

$$[x_{LU}(i\omega)] = [A(i\omega)]^{-1}[B_{NL}(i\omega)] \tag{4}$$

from which the FRFs $[y_{LU}(i\omega)]$ of the linear output vector to unit inputs from the nonlinear block are calculated by

$$[y_{LU}(i\omega)] = [C_{LU}(i\omega)][x_{LU}(i\omega)] + [D_{LU}(i\omega)] \tag{5}$$

To complete the first stage and generate the interim outputs of the linear block in Fig. 2, the linear FD responses of Eqs. (2) and (4) are transformed to TD by

$$\{y_L(t)\} = IFFT\{y_L(i\omega)\} \; ; \; [y_{LU}(t)] = IFFT[y_{LU}(i\omega)] \tag{6}$$

The second stage is performed in the nonlinear block of Fig. 2. The time, t, is set back to zero and a time-marching nonlinear computation of the outputs $\{u_{NL}(t)\}$ of the nonlinear block is performed in consecutive time steps. The outputs $\{y_L(t)\}$ of the linear block are amended in each time step by the convolution integral

$$\{y_{NL}(t)\} = \{y_L(t)\} + \int_0^t [y_{LU}(t-\tau)]\{u_{NL}(\tau)\}d\tau \tag{7}$$

and serve as inputs to the nonlinear functions (*NLF*) in the following time step

$$\{u_{NL}(t)\} = NLF\{y_{NL}(t)\} \tag{8}$$

which may require some sub iterations when $\{u_{NL}(t)\}$ includes direct forces and $\{y_{NL}(t)\}$ includes accelerations. The computation process returns in the third stage to the linear block of Fig. 1. The second-stage output $\{u_{NL}(t)\}$ of Eq. (8) is converted to FD by FFT and the final response is calculated by

$$\{x_{NL}(i\omega)\} = \{x_L(i\omega)\} + [A(i\omega)]^{-1}[B_{NL}(i\omega)]\{u_{NL}(i\omega)\} \tag{9}$$

followed by

$$\{x_{NL}(t)\} = IFFT\{x_{NL}(i\omega)\} \tag{10}$$

This final TD state response may be used for calculating any desired output that is a function of $\{x_{NL}(t)\}$.

The generic transport aircraft (GTA) model of [2] is used here for gust-response numerical example, and later for flutter and LCO analysis. This is a T-tail stick model whose horizontal tail plane (HTP) stiffness has been reduced to yield flutter at velocities below 200m/s. Symmetric analyses were performed with various rotational stiffness values of the elevator actuators. Linear symmetric flutter analysis using *p-k* in MSC/NASTRAN resulted in a bending-torsion flutter at V_f=163m/s, ω_f=12.7Hz, when the actuator was fully attached with its nominal stiffness value of K_{nom}= 2*10⁷N-m/rad. With a disconnected HTP actuator, elevator flutter at V_f=91m/s, ω_f=12.2Hz was obtained. The model was then modified by removing the actuator stiffness and adding a large fictitious moment of inertia at the elevator rotation degree of freedom relative to the HTP when the modal basis was generated. The fictitious inertia is removed in the response analyses, but its effects on the modal basis facilitates high-accuracy variations of the local actuator stiffness over a large range without changing the modal coordinates, as detailed in [2].

Linear gust response analyses were performed at *V*=140m/s with K_{act}= K_{nom} and with K_{act}= 0. The stiffness was added in the first case in two ways: (1) by a zero-order "control loop" that measures the actuator rotation angle, multiplies it by the actuator stiffness defined as a control gain, and applies the resulting moment as a direct control feedback moment applied to the same rotation degree of freedom, with a negative sign; and (2) as an incremental generalized stiffness matrix due to a CELAS2 spring element. The HTP tip acceleration response and the actuator angle with the actuator at its nominal value are shown in Figure 3, with the two

stiffness addition ways exhibiting practically same results. The response with the actuator disconnected (not shown) exhibited a diverging flutter, as expected.
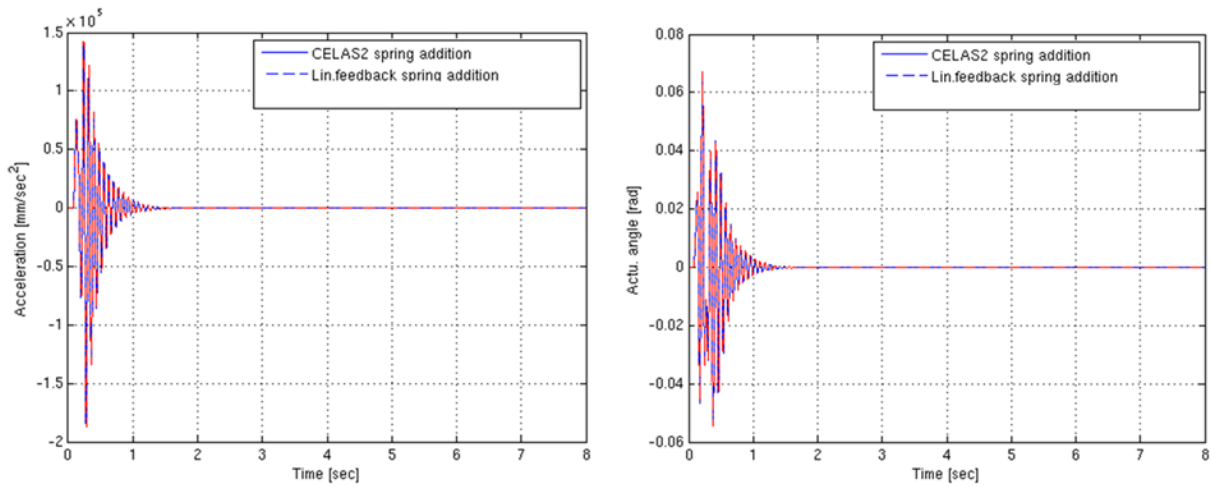

Figure 3: HTP tip acceleration and elevator rotation in response to gust excitation, nominal actuator stiffness

A block diagram of the Dynresp non-linear model for simulating the response to gust excitation with actuator free play of $\delta = \pm 0.02$rad is given in Figure 4. The nonlinear feedback block replace the linear feedback used in way (1) of the linear analysis. The linear plant was also modified by adding the CELAS spring as in way (2) above. The nonlinear feedback block removes the added spring using an equivalent lookup table that forms a nonlinear gain element (NLGAIN). In parallel, the same NLGAIN element is used to add the spring back again, but after the feedback signal passes through a Dynresp-library dead-zone element (DEAZON). The TIMER and SWITCH elements are added to disconnect the feedback after 6 seconds, such that the system becomes stable and returns to zero, as required by the FFT process.

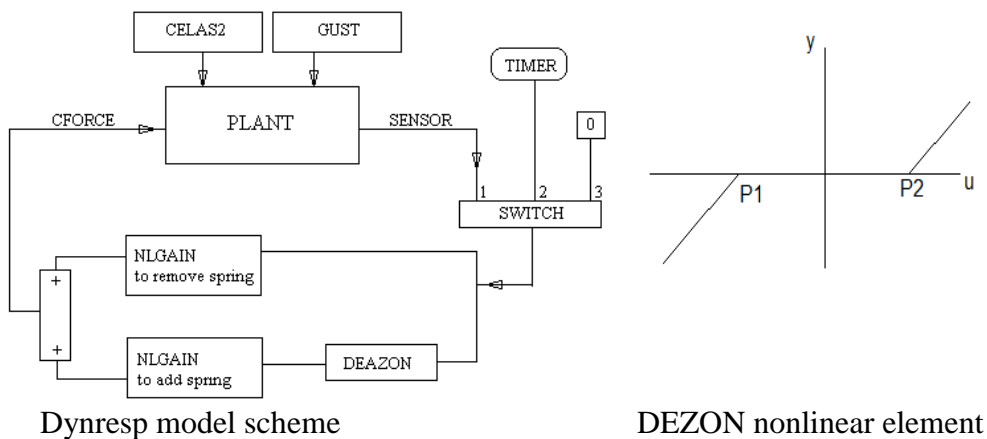Dynresp model scheme   DEZON nonlinear element

Figure 4: Block diagram of the nonlinear model

The resulting nonlinear HTP tip acceleration and actuator rotation angle response are shown in Figure 5. The time histories start with a transient response to the gust excitation, continue with a diverging flutter within the free-play amplitude and exhibit constant-amplitude LCO with the actuator angle amplitude being slightly larger than the free-play amplitude, until the

feedback is disconnected at *t*=6s and the response returns to zero. The modal response may be used for calculating the dynamic loads during LCO using a post-processing loads code such as in the block diagram in Figure 2.
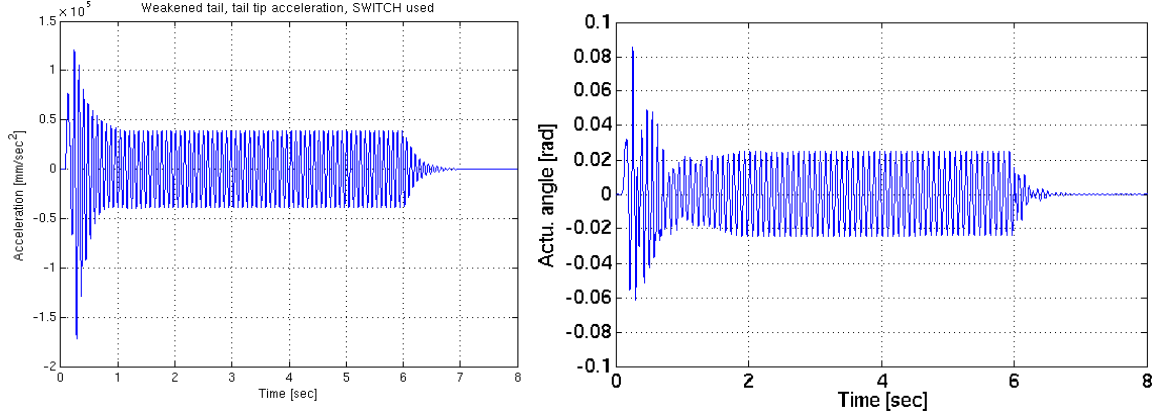

Figure 5: HTP tip acceleration and elevator rotation in response to gust excitation, with actuator free play [2]

Other nonlinear ASE response calculations at Airbus D&S are described in [3], following the computation scheme of Figure 2. The ASE include flight mechanics with nonlinear aerodynamic coefficients, nonlinear gust loads alleviation (GLA) system, aerial refueling boom operation with nonlinear joints and flight-test data, control surface freeplay induced loads, rapture of elastomeric devices during turbopropeller blade loss, and aerodynamic stall at selected panels of the aerodynamic model.

4 AEROSERVOELASTIC STABILITY FORMULATION

4.1 Generalized parametric flutter margin (PFM) method

Linear ASE dynamic stability analysis techniques are aimed at finding the flight conditions that form the flutter boundary at which there is a nontrivial solution to the homogeneous version of Eq. (1), namely

$$\left[A(i\omega)\right]\left\{x_L(i\omega)\right\} = \left\{0\right\} \tag{11}$$

While common flutter solutions are based on finding the conditions at which $\left|A(i\omega)\right| = (0., 0.)$,

The Parametric Flutter Margin (PFM) method is based on FRFs with a stabilizing flutter parameter, p_f, added to the ASE system. Flutter margins are defined by the fraction of p_f that would cause flutter if removed from the modified system. At the flutter boundary, this fraction would be 1.0.

The PFM method was first presented in [5] in its single-input-single-output (SISO) version, in which the selected p_f must be such that its effects can be removed by a SISO control feedback, as demonstrated in Section 4.2. In this paper we first deal with the more general multi-input-multi-output (MIMO) PFM version that was related to in [6]. The flutter onset velocity V_f, the associated flutter frequency ω_f and the respective flutter mode $\left\{x_f(i\omega_f)\right\}$ that solves Eq. (11) characterize the flutter boundary. The only constraint on p_f is defined in a way that yields the FD equation of motion

$$\left[A(i\omega) + p_f B(i\omega)C(i\omega) \right]\{x(i\omega)\} = \left[B(i\omega) \right]\{u(i\omega)\}$$
$$\{y(i\omega)\} = \left[C(i\omega) \right]\{x(i\omega)\} \qquad (12)$$

where the input and output vectors are of the same size. It may be observed that the point (V, ω) at which there is an input vector $\{u_f(i\omega)\}$ that yields the output $\{y_f(i\omega)\}$ that satisfies

$$\{y_f(i\omega)\} = \{u_f(i\omega)\} / p_f \qquad (13)$$

must be a flutter onset point, (V_f, ω_f), because $\{u(i\omega)\}$ in Eq. (12) may then be replaced by $p_f \left[C(i\omega) \right]\{x(i\omega)\}$, which yield Eq. (11). The solution $\{x_f(i\omega)\}$ of Eq. (12) forms in this case a nontrivial solution to Eq. (11). Eqs. (12) and (13), with the real-valued p_f replaced by $1/\lambda(i\omega)$, yield the eigenvalue problem

$$\left[T(i\omega) \right]\{u(i\omega)\} = \lambda(i\omega)\{u(i\omega)\} \qquad (14)$$

where $\qquad \left[T(i\omega) \right] = \left[C(i\omega) \right] \left[A(i\omega) + p_f B(i\omega)C(i\omega) \right]^{-1} \left[B(i\omega) \right].$

The numerical process for finding a flutter onset point is:
1. Define ranges of V and ω, and their increments.
2. For each velocity, solve Eq. (14) for the eigenvalues $\lambda_i(i\omega)$.
3. Plot the magnitude $G_i(\omega)$ and phase $\phi_i(\omega)$ of $\lambda_i(i\omega) / p_f$.
4. Interpolate for $G_i(\omega_{pco})$ where ω_{pco} is the phase-cross-over frequency at which $\phi_i(\omega_{pco}) = 0$. The system is stable when all $G_i(\omega_{pco}) < 1.0$.
5. Plot gain $G_i(\omega_{pco})$ and ω_{pco} vs. V.
6. Interpolate for V_f, at which $G_i(\omega_{pco}) = 1.0$ and extract $\omega_f = \omega_{pco}$.
7. Solve for the flutter mode $\{x_f(i\omega)\}$ of Eq. (11) at (V_f, ω_f).

Flutter margins can be defined in two ways. The first one by the gain $G_i(\omega_{pco})$, in [dB],

$$FM = -20\log\left(G_i(\omega_{pco}) \right)[dB] \qquad (15)$$

that becomes 0dB when $G_i(\omega_{pco}) = 1.0$. The second way is by the increment Δp_f that would bring the system to the flutter boundary

$$\Delta p_f = p_f - \lambda\left(\omega_{pco} \right)_{\max} \qquad (16)$$

Unlike Equation (15), Eq. (16) can be applied with $p_f = 0$, which implies that the eigenvalue analyses associated with different design parameters may be based on the same decomposition of the system matrix inversion $\left[A(i\omega) \right]$. This may be very helpful in design optimization with structural and control variables.

As discussed below, the simplified SISO version of the PFM method may be more efficient in flutter and LCO analyses, various sensitivity studies and flutter tests. The MIMO approach, however, may be of greater value in sensitivity analysis with respect to actual design variables. Reference [6] presents a flutter perturbation study with respect to a factor p_f that multiplies the mass matrix of a refueling pod mounted near the GTA wing's tip. A single MIMO-PFM analysis is shown in [6] to provide the variations in the flutter characteristics for

9

several flutter mechanisms over a selected velocity range. The results are show in [6] to be practically identical to those obtained in numerous MSC/NASTRAN flutter runs.

Another application of the MIMO-PFM method in [6] is for calculating classic "V-g plots" of the variations of aeroelastic frequency and damping vs. velocity, which may be very instrumental in certification documents and in comparing PFM results with classic ones. This was done by defining P_f as a structural damping coefficient. With the modal displacements in $\{x(i\omega)\}$ used as "sensors", and the distribution matrices in Eq. (12) being $[B_f(i\omega)]=[I]$ and $[C_f(i\omega)]=i[K_{hh}]$, $[A(i\omega)]$ is supplemented with an extra modal damping matrix $ip_f[K_{hh}]$. The resulting ΔP_f of Eq. (16) is the damping coefficient g needed to be added to the nominal system for making it neutrally stable, which agrees with the V-g-plot concept. Figure 6 compares the MIMO-PFM results with those obtained with p-k. The same flutter point (at $g=0$) is obtained in both methods and the curve variations are similar. There are slight differences between the damping curves because the added g-related damping term in NASTRAN's p-k application [12] involves the aerodynamic matrix as well.
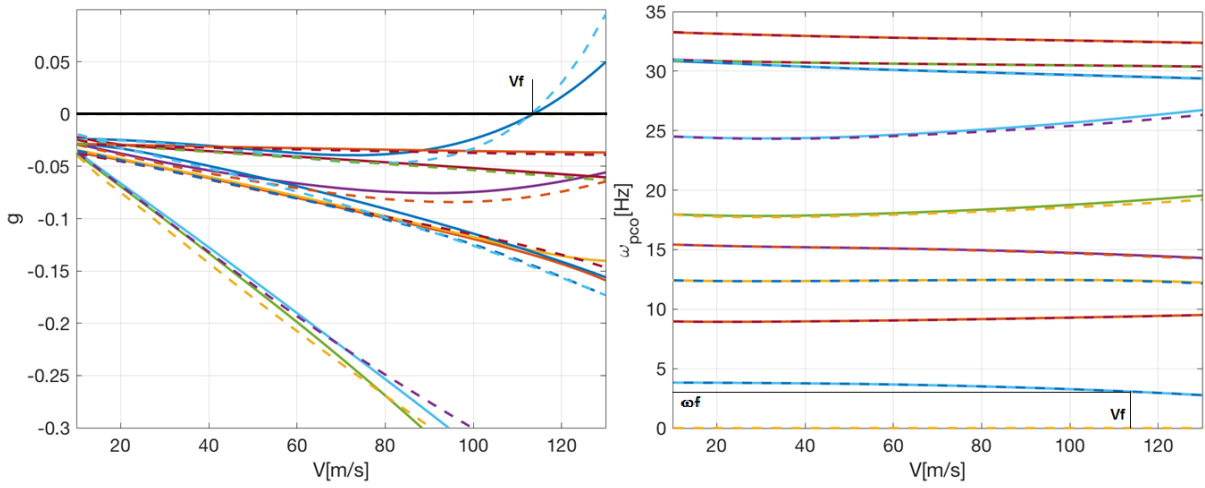

Figure 6: *V-g* plots computed by MIMO-PFM (solid) and *p-k* (dashed), taken from [6]

4.2 Linear SISO-PFM method

When the flutter parameter is limited to those that can be expresses by SISO feedback loops, the incremental $\left[p_f \{B(i\omega)\} \lfloor C(i\omega) \rfloor \right]$ matrix in Eq. (12) is now of rank1. This allows the solution process to be based more efficiently on SISO dynamic response functions without resorting to eigenvalue analysis. In addition, being combined with the IOM method, the ASE stability analysis can be easily expanded to a nonlinear one yielding LCO. Other important applications of the IOM-PFM scheme are in performing safe flutter tests and in CFD-based FSI, as discussed in the following sections.

The SISO-PFM method was originally presented in [5]. It is easy to see that if the open control loop in Eq. (12) is closed by the SISO gain

$$u_f\left(i\omega\right) = p_f\,y_f\left(i\omega\right)$$

(17)

the homogeneous equation (11) is obtained, which implies that the interpolated velocity-frequency pair for which Eq. (17) is satisfied forms the flutter velocity V_f and the flutter frequency ω_f.

The selected p_f and the associated single output and single input parameters of Eq. (12) yield frequency response functions to sinusoidal inputs of amplitude $u_f(i\omega) = 1.0$. The FRFs are presented as Bode plots by their gain and phase variations with frequency

$$G(\omega) = 20\log|P_f y_f(i\omega)|[dB]; \quad \Phi(\omega) = \angle\big(P_f y_f(i\omega)\big)[\deg] \tag{18}$$

The Bode plots are generated for selected points along a line in the flight envelop. The points can be of various air velocities at constant altitude, and various altitudes along a constant Mach line. We assume here a search for non-match flutter conditions at constant altitude and Mach number. The phase functions at the various flight velocities are used for defining the phase crossover frequencies ω_{pco} at which $\Phi(\omega_{pco}) = \pm 360^o n$. These values, and the associated parametric flutter margins $PFM = -G(\omega_{pco})$.

The GTA model of Section 3 is used here for demonstrating the SISO-PFM flutter, LCO and perturbation analyses with respect to the elevator actuator, based on the numerical examples in [5, 6]. The PFM model is based on the model of Section 3. A control system that represents the actuator stiffness is shown in Figure 7. It reflects the baseline nominal stiffness in the model, K_{nom}, and the large actuator stiffness, $p_f = 4*10^7$N-m/rad used as the flutter parameter. The two stiffness values are combined for a single actuator that is connected symmetrically to the two elevators. A linear flutter analysis was first performed to find the free elevator flutter velocity with $K_{nom}=0$ and $p_f=4*10^7$N-m/rad. The resulting gain and phase Bode plots are shown in Figure 8. All the corresponding phase cross-over frequencies and the associated parametric flutter margins (PFM) vs. velocity, calculated in Dynresp, are shown in Figure 9. The branch of smallest flutter margins crosses the zero-dB line at V_f=91.1 m/s, ω_f=12.2 Hz. The interpolated complex response vector at this flutter onset point, normalized to maximal value of (1.0; 0.0), is the flutter mode $\{x_f(i\omega_f)\}$.
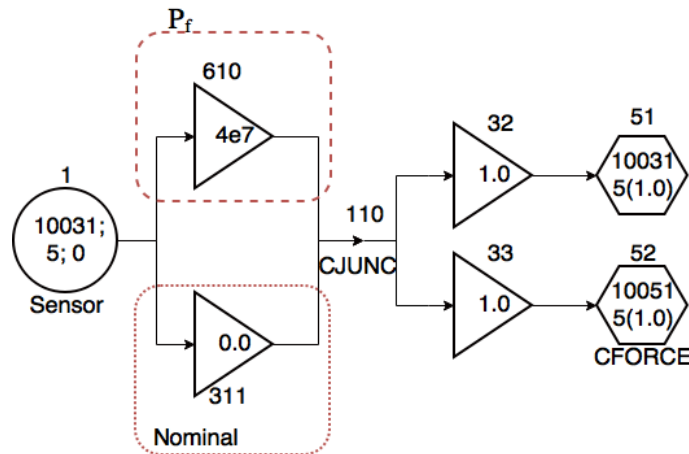

Figure 7: Control gains that represent the actuator stiffness
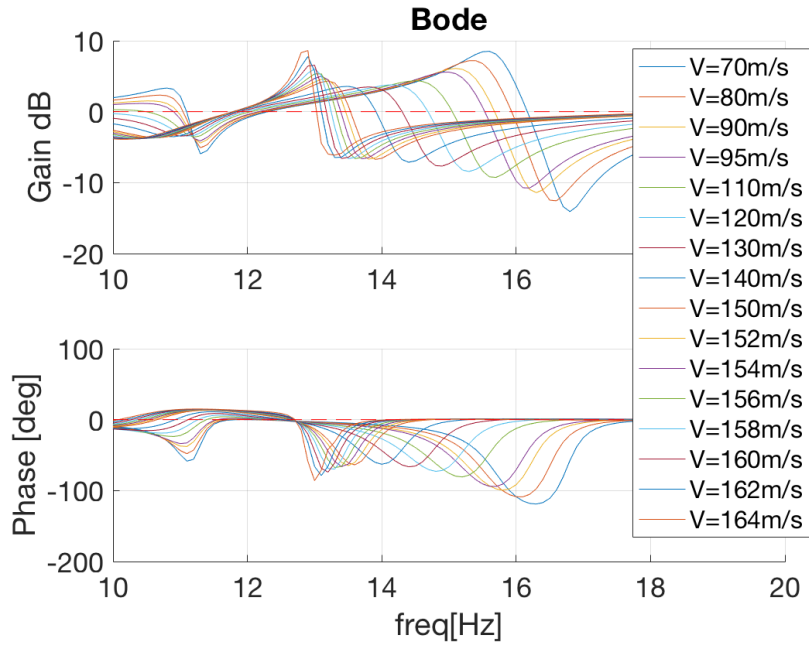
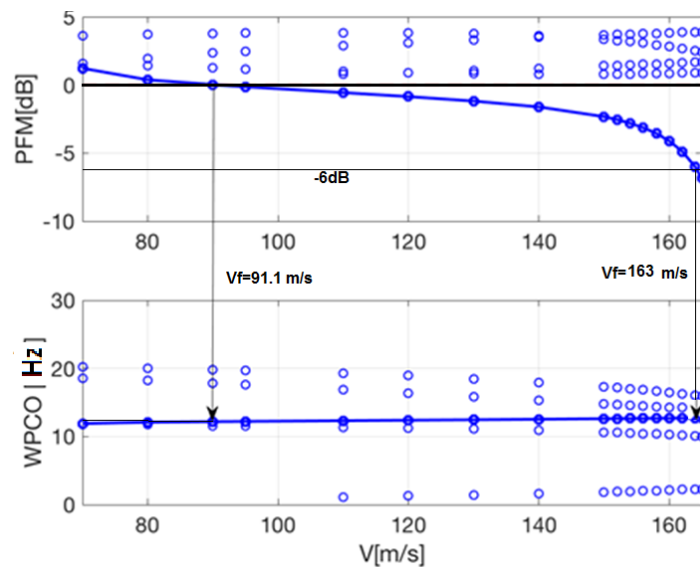Figure 8: Flutter gain and phase plots vs. frequency

Figure 9: Phase cross-over flutter margins and frequencies vs. velocity

An important advantage of the SISO-PFM method is that the baseline PFM plot can be used for an extensive perturbation analysis in which the flutter parameter varies over a wide range. The perturbation analysis can be performed by simply moving the 0dB line in the PFM plot of Fig. 9 vertically. Moving it down by 6dB is equivalent to repeating the PFM analysis with $p_f/2=2*10^7$N-m/rad becoming part of the system, and the other half of is used as the new p_f. Now, with the flutter velocity defined by the PFM crossing of the -6dB line, the flutter velocity becomes 163 m/s. Since the $p_f/2$ value is that of the original actuator, we just found the flutter characteristics of the GTA model with a fully connected actuator. In this way, the same plot can be used to extract the entire variation of flutter characteristics vs. actuator stiffness by simply moving the 0dB line up or down.

The Dynresp framework provides for using any ASE response parameter, which can be defined as a direct or frequency-dependent linear combination of the system states and control inputs, as a "sensor". It also allows the use actuator commands and other control inputs, as well as direct discrete and generalized forces, as feedback inputs. This facilitates the application of numerous parameters, such as discrete masses [7-9], modal damping [6], aerodynamic coefficients and local stresses as flutter parameters p_f, with respect to which flutter analysis is performed. When the selected p_f is an actual control gain, the stability analysis in Dynresp provide the standard Nyquist SISO control gain and phase margins [13], with aeroelastic effects of course.

4.3 Nonlinear SISO-PFM method

Nonlinear LCO analysis can be performed in Dynresp in various ways. One way is by running nonlinear response simulation, such as the free-play one done in [2] and in Section 3 above, and searching for diverging or LCO response. This solution may yield the most accurate result, but it might also be very inefficient and with numerical difficulties in dealing with diverging systems. Alternatively, the SISO-PFM method can be based on dynamic response functions with nonlinear elements, performed with different excitation levels. Harmonic Balance (HB) techniques can be used to account for the inter-frequency effects due to non-harmonic response functions [5].

A special case is when the only nonlinearity is in the SISO feedback loop that defines p_f [6]. Linear FRFs can be calculated in this case for extracting $y_L(t)$ and $y_{LU}(t)$ of Eq. (6), and then used for calculating the nonlinear feedback in frequency-domain terms as function of the vibration level. This process, detailed in [6], is very efficient when used with 1st-order HB, which is equivalent to the Describing-Function (DF) technique. A comparison between LCO response of the actuator spring in the GTA example of Section 2, obtained by full IOM solutions [2], by the 1st-order HB [5] and the DF [6] special-case solutions, is given in Figure 10. The normalized LCO amplitudes θ/δ and the LCO frequency vs. velocity plots indicate that LCO starts at the free-elevator flutter velocity of 91.1 m/s, and approached infinity at the fully-connected flutter velocity of 163 m/s. It is clear that the efficient solutions are similar to the time simulation ones and slightly more conservative.
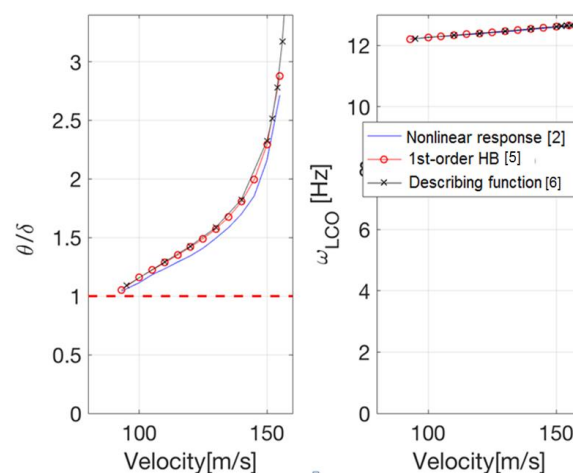

Figure 10: LCO amplitudes by nonlinear IOM response [2], 1st-order HB and describing function [6]

The sensor definitions in Dynresp facilitate the inclusion of section loads, such that they can be monitored in the simulation runs. The related sensors are based in the following example of stiffness properties of the CBAR element in NASTRAN. Alternatively, full net-load distributions and associated section loads can be obtained by post processing the modal and control-surface response functions using load codes such as Dynload in Fig. 2. The post processing can be based on the mode-displacement (MD) approach, which is also used in the CBAR sensor definition, or on the more accurate summation-of-force (SOF) approach.

The CBAR loads in the DF LCO simulations of Fig. 10 are compared in Fig. 11 with the HTP root loads calculated using the SOF approach. There is 5.3% difference between the two shear force amplitudes and 3.4% difference between the two bending moment amplitudes. Considering the fact that the modes taken into account contain only a few symmetric elastic modes with significant HTP participation, this comparison is quite good. The SOF loads are more accurate than the MD ones as they converge faster with the number of modes taken into account.
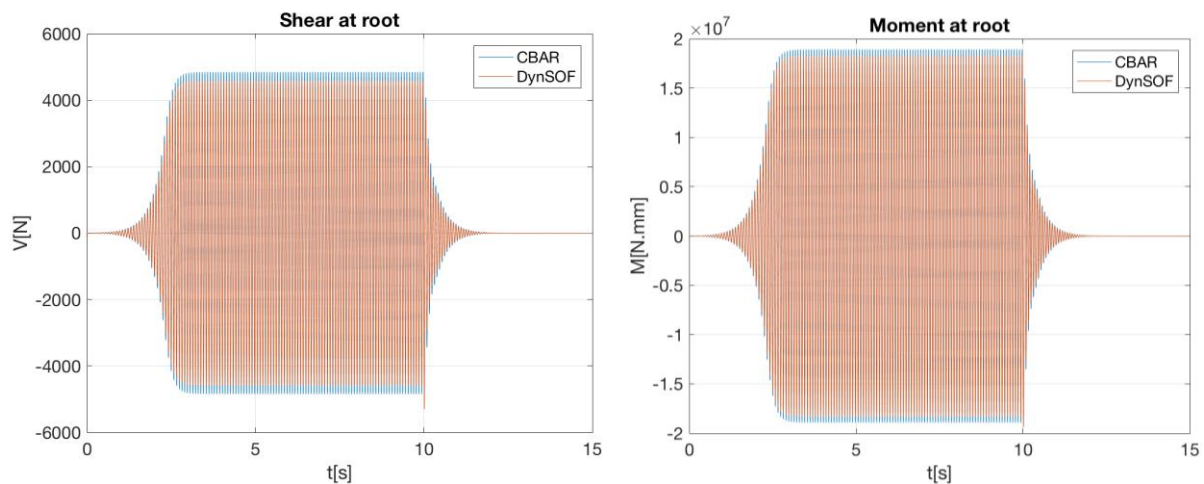

Figure 11: Shear force and bending moment at HTP root in LCO, by CBAR output and SOF

5 AERODYNAMIC MORPHING AND NONLINEARITY

Common industrial aeroelastic response and dynamic loads codes assume fixed flight conditions and aerodynamic shape, except for small elastic deformations and control-surface deflections. Linear unsteady aerodynamic coefficients usually account for the aerodynamic load changes due to the associated shape changes and regulation gust excitation. The IOM application in the Dynresp framework provides for unconventional response simulations with morphing configurations [14], rapid changes of flight conditions [15], wake encounter [16] and CFD-based unsteady aerodynamics [17,18]. The gust response simulation of a morphing configuration in [14] exhibits the key features in Dynresp that facilitated these analyses. It is of an air vehicle whose symmetric aeroelastic model is divided into two substructures, body-tail, and wing. The wing rotates from zero sweep angle to 60 deg in one second. Aeroelastic response analysis was performed to study the wing loads when the vehicle is excited by a uniform discrete vertical gust while the wing changes its sweep angle. The time history of the sweep angle is assumed to be known. Modal coupling between the two substructures is performed at each time point in a way that satisfies the boundary interface displacements and slopes. The coupling equations are developed in [14] such that the wing rigid-boy modal coordinates are eliminated and the remaining generalized mass matrix changes continuously. The incremental mass coupling terms are introduced in the Dynresp run by a feedback loop

that reads generalized accelerations, multiplies them by the time-dependent mass coupling terms and applies the resulting generalized forces, with reversed signs, as nonlinear inputs in $\{u_{NL}(i\omega)\}$ of Eq. (9).

The aerodynamic panel model also changes during the morphing process, which affects the generalized aerodynamic forces. The linear ZAERO model is first generated with the aircraft geometry at $\Lambda = 0$ with the respective modal matrix $\Phi_h(0)$. The aerodynamic matrices at other sweep angles are also generated in preparation for the linear run at several sweep angles between 0 and 60 *deg*. The unsteady modal matrices and gust vectors $Q_{hhi}(i\omega)$ and $Q_{hGi}(i\omega)$ are generated for the selected sweep angles considering the affected aerodynamic model and structural modes $\Phi_h(\Lambda_i)$. They are used in Dynresp for defining the linear outputs of Eq. (3) as

$$
\begin{Bmatrix} y_{h1_L}(i\omega) \\ y_{h2_L}(i\omega) \\ \vdots \\ y_{hn_L}(i\omega) \\ y_{acc_L}(i\omega) \end{Bmatrix} = \begin{bmatrix} Q_{hh1}(i\omega) \\ Q_{hh2}(i\omega) \\ \vdots \\ Q_{hhn}(i\omega) \\ -\omega^2 I \end{bmatrix} \{X_L(i\omega)\} + \begin{Bmatrix} Q_{hG1}(i\omega) \\ Q_{hG2}(i\omega) \\ \vdots \\ Q_{hGn}(i\omega) \\ 0 \end{Bmatrix} \frac{w_G(i\omega)}{V} \tag{19}
$$

such that $\{y_{hi_L}(i\omega)\}$ reflects the generalized unsteady aerodynamic forces if Λ would change to Λ_i and $\{y_{acc_L}(i\omega)\}$ is the vector of generalized accelerations needed for the modal coupling. Similarly to the aerodynamic matrices in Eq. (1), the FD coefficient matrices in Eq. (22) are defined at the selected frequency values and interpolated during the FD solution to all the frequency values at which Eq. (1) is solved with discrete gust inputs.

Once the solution $\{X_L(i\omega)\}$ and the output $\{y_L(i\omega)\}$ are calculated, they are transformed to TD, $\{X_L(t)\}$ and $\{y_L(t)\}$, using IFFT. In addition, the frequency response matrix $[y_{LU}(i\omega)]$ is calculated using Eqs. (4) and (5) with the inputs being unit-amplitude generalized forces and the outputs are those of Eq. (19). IFFT of $[y_{LU}(i\omega)]$ yields the respective impulse response matrix $[y_{LU}(t)]$ for the convolution of Eq. (7), performed with $\{u_{NL}(\tau)\}$

$$
\{u_{NL}(t)\} = -[\Delta M_{hh}(\Lambda)]\{y_{acc_{NL}}(t)\} - q\{\Delta y_{h_{NL}}(t)\} \tag{20}
$$

where the sweep angle Λ is a prescribed function of t. The generalized aerodynamic feedback $\{\Delta y_{h_{NL}}(t)\}$ is interpolated from the aerodynamic outputs of $\{y_{NL}(t)\}$ in Eq. (7).

All the element of the linear aeroelastic model, including the FD coefficient matrices in Eq. (19), were constructed with standard elements of the Dynresp code. A special user-defined function (UDF) was programmed for the interpolation of the nonlinear inertial and aerodynamic feedback forces of Eq. (20). The Dynresp framework provides for adding such UDFs to the library of nonlinear elements at the user site, without the need to recompile the entire code. Sample wing-root section loads and wing-tip acceleration, taken from the gust-response analysis presented in [14] are shown in Fig. 12. The plots demonstrate that the gust loads may be affected significantly by the sweep angle and by morphing rate and direction.
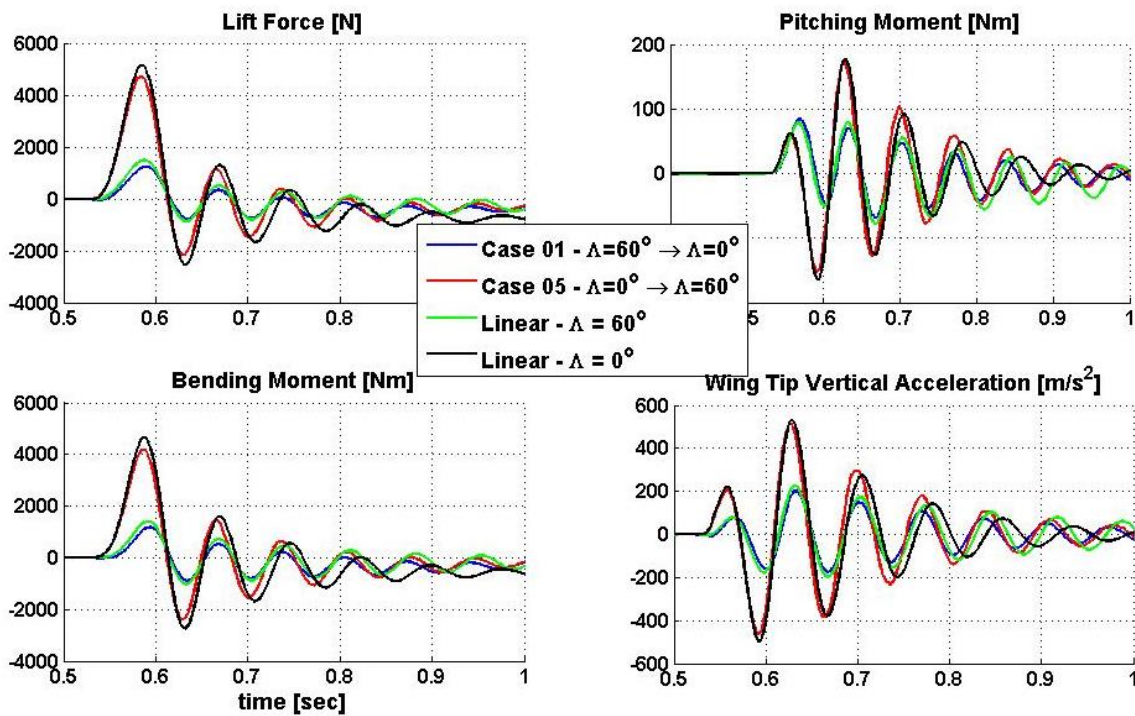
Figure 12: Wing-root section loads and wing-tip vertical acceleration [14]

The response simulations in [15] included rapid change in the flight condition, with the vehicle accelerating from rest to Mach 2.0 in a few seconds, together with a significant change of mass during the acceleration, nonlinear structural joints, and misaligned follower thrust force. The treatment of the velocity and mass changes is done with sensors and nonlinear feedback terms similar to those of Eqs. (19) and (20), with the special UDF connecting between them includes a gain that expresses the changes in the dynamic pressure q in Eq. (20). The nonlinear joint stiffness was introduced with a feedback loop similar to the one in Fig. 4, with a nonlinear lookup-table gain element of Dynresp library replacing the DEZON element. The lateral component of the thrust misalignment force was also introduced by a nonlinear library element based on the modal deformations.

The wake-encounter analysis in [16] was performed to analyze the dynamic loads on an aircraft crossing its own wake or that of another aircraft. It requires a preliminary analysis that maps the wake velocities in space and extracts the induced wake incidence angles at the control points of the aerodynamic boxes, for any encounter penetration geometry. The introduction the wake incidence angles is facilitated in Dynresp by its ability to define separate gust velocities to every aerodynamic model box or group of boxes. The computation process was validated at Airbus D&H [16] by comparison of A400M flight-test section loads measurements with the measured aircraft penetrating the wake of another aircraft. Since the position of the wake penetration was not known with sufficient accuracy, it was optimized to provide a good overall comparison of the numerical and experimental results. A block diagram of the optimization process and a sample comparison wing-root bending moments are given in Fig. 13.
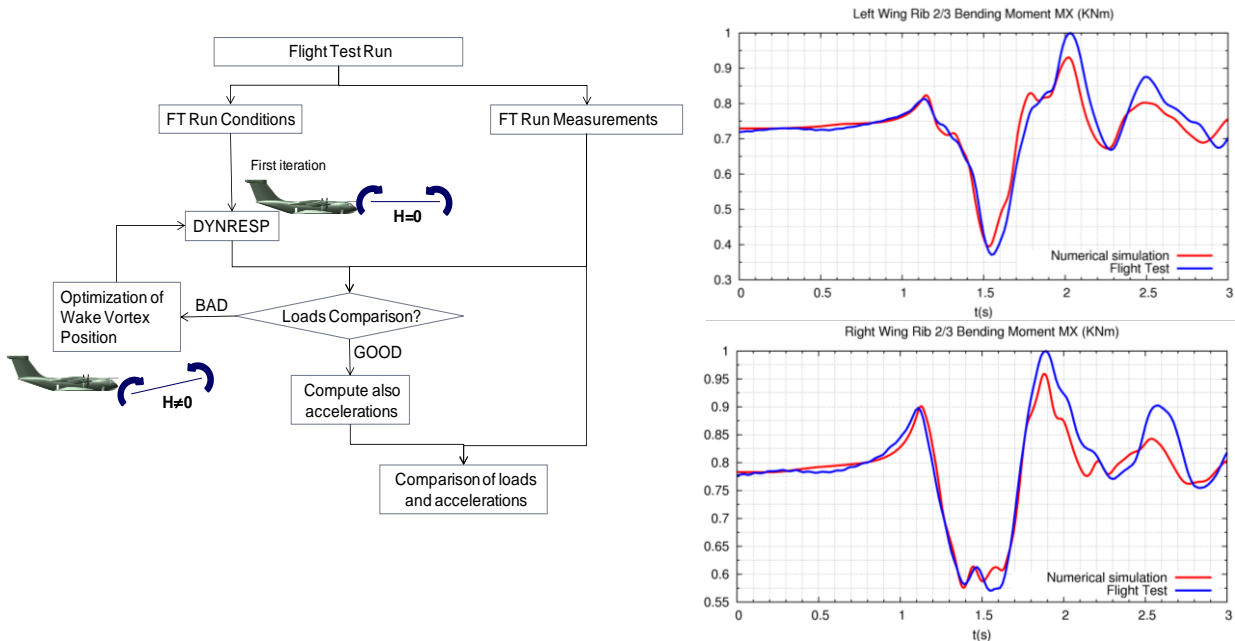
16

Figure 13: Numerical simulations of A400M wing root bending moment in wake vortex encounter compared with flight test results (encounter at an angle of $\psi=40°$) [16]

A rapidly growing usage of Dynresp is in integration with unsteady CFD codes for FSI. The basic idea is that the ASE simulation and the CFD codes should be separated, with an interface module. In this way, each code is developed and maintained by its own professionals that typically have very different backgrounds. The Dynresp interface module with generic CFD codes is marked in the lower-right part of the block diagram of Fig. 1. It indicates three different coupling procedures with CFD codes: (a) via CFD-based linearized generalized unsteady aerodynamic force coefficient matrices $[Qhh(i\omega)]$; (b) with a tight-coupling procedure; and (c) with a loose-coupling procedure.

The procedures for extracting $[Qhh(i\omega)]$ matrices for CFD codes , see for example [17], are beyond the scope of this paper. Once generated, they may replace the entire input aerodynamic matrices for Dynresp, or only some portions of them. After the ASE characteristics are studied using Dynresp, the CFD-based modal and frequency contents may be updated.

The Dynresp nonlinear UDF module in Fig. 1 was developed for tight coupling with any CFD framework that can handle projected structural modes to its surface grid, import modal displacements, solve for time-marching surface pressure distributions, calculate generalized forces, and export them at every time step. It reads the time-domain generalized aerodynamic forces of Dynresp, update them according to those imported from the FSI files, and exports to them the current modal displacements for a subsequent CFD time step. While the UDF is fixed and belongs to the Dynresp environment, the FSI interaction procedure and data files are customized according to the CFD procedures.

6 SAFE FLUTTER TESTS

Flight and wind-tunnel flutter tests are conducted during the development of flight vehicles to demonstrate that they are free from flutter over their entire operation envelope. Various

experimental methods may be applied to validate the numerical stability models and identify the flutter boundaries. However, for obvious safety reasons, the tests are conducted very carefully such that flutter would not occur, which make the tests expensive, risky and time consuming. The idea of using the PFM approach to perform safer flutter tests was first raised in [7]. A procedure was presented in which the tests are performed with a SISO element added to the aeroelastic system in a way that expands the flutter envelope. Tests are then performed to positively identify the nominal flutter conditions while testing the stabilized article.

Three proof-of-concept wind-tunnel tests [7-9] have already been performed and published. The first one [7] was not planned for this purpose. The tests were carried out as part of the EU-funded Clean-Sky GLAMOUR project [19]. A 1:6 half-span, floor-sliding, aeroelastically-scaled model of the aircraft was built and mounted vertically downstream of specially designed gust generators, as depicted in Figure 14. Two wing ailerons and one T-tail elevator, driven by mini actuators were used for gust alleviation based on various response measurements at CG, wing tips and elevator, a virtual AOA sensor and control-surface rotations.
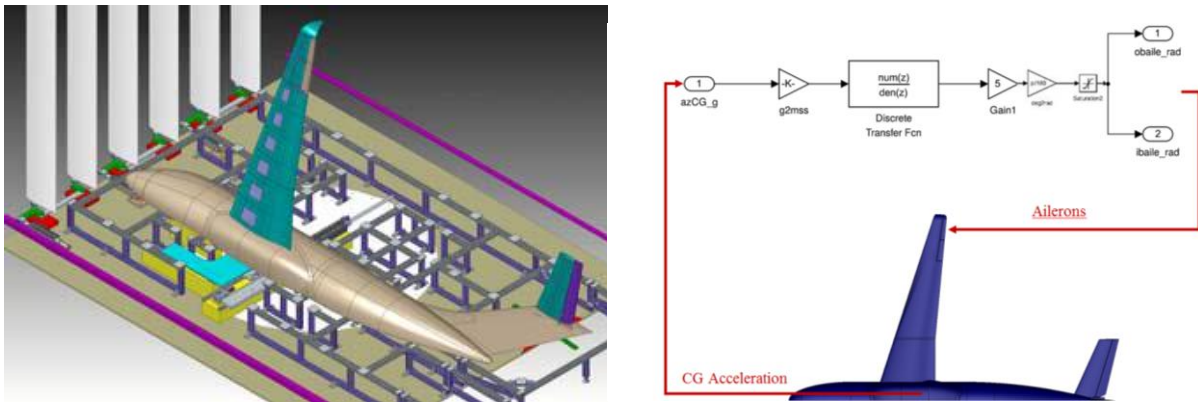

Figure 14: Wind-tunnel model, gust generators, the dummy floor internal structure and the GLA1 control scheme [19]

Open-loop flutter tests were carried out using sinusoidal excitation sweeps obtained by commanding the aileron in the range of 0.3 to $2.5\omega_l$, where ω_l is the natural frequency of the first wing-bending mode. Experimental modal analysis verified that the model is free from flutter in the entire tunnel velocity range. However, flutter started to develop when one of the gust alleviation loop was closed, which caused an immediate disconnection of the control feedback. The open-loop test results and the PFM method provided us with the opportunity of identifying closed-loop flutter events from the open-loop test results. The flutter parameter, p_f, was selected to be the closed-loop control gain, *Gain1*, of the GLA1 control loop that relates the aileron input to the measured CG acceleration. This selection yields the gain margins associated with *GAIN1*. The PFM analysis did not indicate flutter in the searched envelope. However, with p_f=- *Gain1*, the PFM gain and frequency plots of Fig. 15 indicated flutter in the middle of the test velocity rang. An excellent agreement is shown in Fig. 15 between the plots based on the experimental results and those extracted from the numerical aeroelastic model.
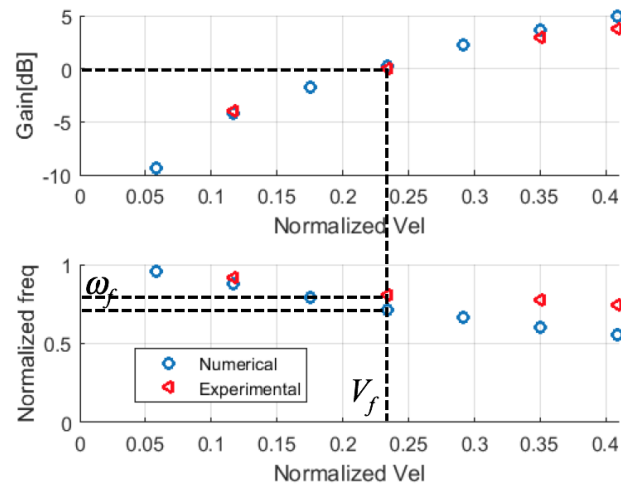
Figure 15: Cross-over frequency and flutter gain variations with velocity

The two other PFM wind-tunnel flutter tests were performed with a single mass serving as the stabilizing element. The first one was a 2D test [8] conducted at TUDelft with a wing section connected at its rotation axis to the ground through heave and pitch spring. Preliminary tests exhibited flutter within the tunnel velocity range. A mass, m_f, was then connected to the rotation axis at a forward position with a loads cell for measuring the impulsive normal hammer inputs, and an accelerometer for measuring the normal acceleration. FFT analysis of the input and output signals resulted in Bode plots from which the no-mass flutter velocity was identified using the PFM analysis. Even though the results were noisy, the nominal flutter velocities were identified for several spring combinations with less than 5% errors.

The third PFM test was conducted at Technion with a 3D wing model, whose nominal flutter characteristics were already known, with a mass added at the tip store, in a forward position, serving as stabilizing element. The excitation was performed by tying the mass to a fishing chord, pulling it with a known static force, and cutting the chord at several velocities. Here again, FFT analysis and PFM plots predicted the flutter velocity of the nominal system, from flutter tests of the stabilized one, with less than 5% errors.

7 CONCLUSIONS

The Dynresp framework for aeroservoelastic response and stability module has been demonstrated in many industrial and research applications to yield all the numerical data necessary for dynamic stability characteristics and dynamic loads for certification of modern aircraft. The linear results has been shown by various examples in technical publications to be practically identical to other commonly used software packages, when performed with same input parameters and analysis requirements. The unified frequency-domain formulation of the response equations with various excitation means, control-system integration options and the expanded simulation output parameters provide for convenient operation of the software in all it disciplines for both deterministic and stochastic analyses. The implemented IOM approach facilitates the inclusion of nonlinear elements at any appropriate complexity level, from simple lookup tables to the interaction with high-fidelity codes. The nonlinear module facilitates the simulation a large variety of operational events such as morphing, system malfunctions and changes in flight conditions. Loads perturbation analyses are easily performed as many parametric changes may be adequately introduced without changing the modal and aerodynamic data base. The PFM stability analysis is virtually based on the same system modeling and equations of motion. The more general MIMO-PFM version may be

more useful in automated design studies and in generating classical V-g plots. The SISO-PFM, however, is more efficient and useful in regular flutter and control-margin analyses, and in investigating nonlinear effects on flutter and LCO. Preliminary investigations have already demonstrated the potential in using the IOM-PFM integrated software for high-fidelity fluid-structure interaction analysis and in enhancing the safety of flutter flight tests.

8 REFERENCES

[1] Karpel, M., "Increased-Order Modeling Framework for Nonlinear Aeroservoelastic Analysis," Proceedings of the International Forum on Aeroelasticity and Structural Dynamics, Paper No. 2011-71, Paris, France, June 2011.

[2] Karpel, M., Shousterman, A., Maderuelo, C., and Climent, H., "Dynamic Aeroservoelastic Response with Nonlinear Structural Elements," *AIAA Journal*, Vol. 53, No. 11, 2015, pp. 3233-3239.

[3] Reyes, M., Climent, H., Karpel, M, Arevalo, F. and Maderuelo, C., "Examples of increased-order aeroservoelastic modeling," *CAES Aeronautical Journal*, Jan. 2019, doi: 10.1007/s13272-019-00361-w.

[4] Drachinsky, A., Shitrit, S., Arad, E. Roizner, F., and Karpel, M.,"Nonlinear CFD-based dynamic aeroelastic response of a fin with structural hysteresis", Proceedings of Israel Annual Conference on Aerospace Sciences IACAS, March 2018.

[5] Roizner, F., and Karpel, M., "Parametric Flutter Margin Method for Aeroservoelastic Stability Analysis", *AIAA Journal*, Vol. 56, No. 3, 2018, pp. 1011-1022.

[6] Roizner, F. and Karpel, M., "Sensitivity of Aeroservoelastic Stability Characteristics Using Parametric Flutter Margins," *Journal of Aircraft*, March 2019, article in advance pp. 1-11 , doi: 10.2514/1.C035286.

[7] M. Karpel and F. Roizner, "Towards Flutter-Boundary Tests with Controlled Vibration Levels", proceedings of the 57th IACAS Conference, Tel Aviv, Israel, 2017.

[8] Sodja, J., Roizner, F., De Breuker, R., and Karpel, M., "Experimental Characterisation of Flutter and Divergence of 2D wing Section with Stabilized Response," ELSEVIER Journal of Aerospace Science and Technology, No. 78, 2018, pp.542-552.

[9] Roizner, F., Raveh, D. E. and Karpel, M., "Safe Flutter Tests Using Parametric Flutter Margins," *Journal of Aircraft*, Vol. 56, No. 1, 2019, pp.228-238, doi: 10.2514/1.C035045.

[10] Karpel, M, Shousterman, A., Reyes, M., and Climent, H., "Dynamic Response to Wake Encounter," AIAA Paper 2013-1921, presented at the SDM conference, Boston, MS, April 2013.

[11] Karpel, M., Shousterman, A. and Mindelis, Y., "Rigid-Body Issues in FFT-Based Dynamic Loads Analysis with Aeroservoelastic Nonlinearities", AIAA Paper 2414- 53rd AIAA/ASME/ASCE/AHS/ASC Structures, Structural Dynamics, and Materials Conference, Honolulu, HW, April 2012.

[12] Rodden,W. P., Harder,R. L., and Bellinger, E. D., "Aeroelastic Addition to NASTRAN," NASA CR 3094, 1979.

[13] Ogata, K., *Modern Control Engineering,* 4th ed., Prentice-Hall, Upper Saddle River, NJ, USA, 2002.

[14] Karpel, M., Romm, A., Reyes, M., and Climent, H., "Aircraft Dynamic Loads with Varying Geometry and Flight Mechanics Effects," Proceedings of the International Forum on Aeroelasticity and Structural Dynamics, Paper No. 2015-183, Saint Petersburg, Russia, June 2015.

[15] Karpel, M., Shousterman, A., Livshits, D. and Yujelevski, Y., "Dynamic Response of Accelerated Rocket with Nonlinear Effects," Proceedings of the 54th IACAS Conference, Tel Aviv, Israel, 2014.

[16] Claverías, S., Cerezo, J., Torralba, M.A., Reyes, M., Climent, H. and Karpel, M., "Dynamic Loads in Response to Wake Encounter," Proceedings of the 54th IACAS Conference, Tel Aviv, Israel, 2014.

[17] Karpel, M., Roizner, F., Carrese R., and Marzocca, P., "Parametric Flutter Margin of Twin Tail Configuration in Wing-Generated Buffet," Proceedings of the International Forum on Aeroelasticity and Structural Dynamics, Paper No. 2017-106, Como, Italy, June 2017.

[18] Roizner, F., Karpel, M., Carrese R., Joseph, N. and Marzocca, P., "Parametric Flutter Margin Analysis with CFD-Based Aerodynamics," AIAA 2018-0704, proceedings of the AIAA SciTech Forum, Orlando, FA, Jan. 2018.

[19] Ricci, S., De Gaspari, A., Fonte, F., Riccobene, L., Toffol, F., Mantegazza, P., Karpel, M., Roizner, F., Wiberman, R., Weiss, M., Cooper, J.E., Howcroft, C., Calderon1, D., "Design and Wind Tunnel Test Validation of Gust Load Alleviation Systems," AIAA-2017-1818, presented at the SciTech conference, Dallas, TX, January 2017.

COPYRIGHT STATEMENT